Check for updates

ADVANCED OPTICAL MATERIALS
www.advopticalmat.de

Fusion of Selenium-Embedded Multi-Resonance Units Toward Narrowband Emission and Fast Triplet-Singlet Exciton Conversion

Jibiao Jin, Mei Chen, He Jiang, Baohua Zhang, Zhiyuan Xie, and Wai-Yeung Wong**

Developing multi-resonance thermally activated fluorescence (MR-TADF) emitters with both fast reverse intersystem crossing (RISC) rate and narrow emission bandwidth still remains a formidable challenge. Herein, a design strategy of fused MR skeleton containing heavy chalcogen (sulfur or selenium) for high-performance MR-TADF molecules is developed. Impressively, Se-embedded emitter (DSeBN) shows extremely narrow full width at half maximum (FWHM) value of 16 nm and ultrafast RISC rate constant up to 2.0×10^6 s^{-1}. The organic light-emitting diode (OLED) based on this emitter exhibits excellent performance parameters with extremely narrow FWHM of 17 nm and high external quantum efficiency (EQE) of 35.31%. Significantly, much suppressed efficiency roll-off is achieved, in which the EQE still stayed at 32.47% and 25.05% at the luminance of 100 and 1000 cd m^{-2}, respectively. These results represent the state-of-the-art device performance in terms of efficiency and FWHM, shedding new light on the development of practical MR-TADF emitters.

1. Introduction

Thermally activated delayed fluorescence (TADF) emitters that acted as the candidates for the third generation organic light-emitting diodes (OLEDs) have received considerable attention from the perspectives of academic research and commercial application.[1–6] To realize high-performance TADF molecules, small energy gap between the singlet and triplet states (ΔE_{ST}) and highly emissive efficiency as well as narrow emission profile are necessary requirements.[7–9] However, small ΔE_{ST} generally benefits from the twist donor-acceptor (D-A) configuration for the separated distributions of the highest occupied molecular orbital (HOMO) and the lowest unoccupied molecular orbital (LUMO), which leads to a reduced oscillator strength with a low emission efficiency and an enlarged structural reorganization with a broad emission profile.[10–12] The typical full width at half maximum (FWHM) of TADF molecules with D-A configuration exceeds 70 nm, which needs to cut off the margin region by the optical filter or microcavity for high-definition displays, thus leading to undesired significant energy loss.

In 2016, Hatakeyama et al. developed a kind of multi-resonance TADF (MR-TADF) molecules by using the multi-resonance effect of electron-withdrawing boron (B) and electron-donating nitrogen (N) atoms, giving rise to the alternative distributions of HOMO and LUMO on the atomic level.[13] Moreover, the N and B atoms were embedded into a rigid polycyclic aromatic framework, resulting in a small structural reorganization for a narrowband emission. With such characters, small ΔE_{ST} and high efficiency as well as narrowband emission can be integrated in MR-TADF molecules simultaneously, indicating their enormous potential for high-performance electroluminescence (EL) devices.[14–18] However, MR-TADF molecules usually

J. Jin, H. Jiang, W.-Y. Wong
Department of Applied Biology and Chemical Technology and Research Institute for Smart Energy
The Hong Kong Polytechnic University
Hung Hom, Hong Kong, P. R. China
E-mail: wai-yeung.wong@polyu.edu.hk

J. Jin, H. Jiang, W.-Y. Wong
The Hong Kong Polytechnic University Shenzhen Research Institute
Shenzhen 518057, P. R. China

The ORCID identification number(s) for the author(s) of this article can be found under https://doi.org/10.1002/adom.202400794

© 2024 The Author(s). Advanced Optical Materials published by Wiley-VCH GmbH. This is an open access article under the terms of the Creative Commons Attribution License, which permits use, distribution and reproduction in any medium, provided the original work is properly cited.

DOI: 10.1002/adom.202400794

M. Chen, B. Zhang
Center for Advanced Analytical Science
Guangzhou Key Laboratory of Sensing Materials and Devices
Guangdong Engineering Technology Research Center for Photoelectric Sensing Materials and Devices
and School of Chemistry and Chemical Engineering
Guangzhou University
Guangzhou 510006, P. R. China
E-mail: ccbhzhang@gzhu.edu.cn

B. Zhang, Z. Xie
State Key Laboratory of Polymer Physics and Chemistry
Changchun Institute of Applied Chemistry
Chinese Academy of Sciences
Changchun 130022, P. R. China

exhibit unsatisfactory reverse intersystem crossing (RISC) rate because of the small spin-orbit coupling (SOC) matrix elements (<0.1 cm^{-1}) between the singlet and triplet excited states, causing a severe efficiency roll-off of the EL devices.[19–21]

Introducing the heavy atoms, such as sulfur (S) or selenium (Se), into the MR-TADF framework can significantly enhance the SOC values, thereby accelerating the spin-flip process of excitons for the fast RISC rate by heavy-atom effect.[22–24] Brédas et al. theoretically investegated the impact of replacing oxygen atoms with sulfur or selenium atoms on the MR-TADF properties, confirming that the chemical nature and positions of the chalcogen atoms have a crucial impact on the photophysical properties.[25] Yang et al. reported the selenium (Se)-integrated MR-TADF molecules (BNSSe and BNSeSe) whose RISC rate reached 2.6×10^6 s^{-1}. The corresponding OLEDs showed excellent performance with high external quantum effieiceny (EQE) of 36.8% and ultra-low roll-off.[26] Yasuda et al. reported the S/Se doped blue MR-TADF emitter (CzBS and CzBSe), realizing a very large RISC rate constant exceeding 10^8 s^{-1}. The OLED based on CzBSe as the emitter achieved a high maximum EQE of 23.9% and reduced efficiency roll-off, in which the EQEs still stayed at 23.4% and 20.0% at 100 and 1000 cd m^{-2}, respectively.[27] However, the large FWHM value (>30 nm) was observed both in these two strategies. Furthermore, by the fusion of S-embedded MR units, Yasuda et al. developed a MR-TADF emitter (BSBS-Z) with both narrow FWHM value of 22 nm and high EQE of 26.8%.[28] However, the Se-embedded analogue is hardly to synthesize by using the same method but it is more attractive in terms of improving the RISC rate and device performance.

Herein, a design strategy of fusion of S/Se-B-N MR unit was developed by using a one-shot borylation reaction to fabricate high-performance MR-TADF molecules with both extremely narrow FWHM and ultrafast RISC rate. Moreover, six methyl groups were introduced to improve the solubility and aggregation effect which are the common problems of rigid MR-TADF molecules encountered. Such prepared **DSBN** and **DSeBN** exhibit excellent solubility and sky-blue emission peaking at 472 and 473 nm with an extremely narrow FWHM of 18 and 17 nm, respectively. Benefiting from the heavy-atom effect, TADF characteristics were significantly improved, with high delayed fluorescence efficiencies and fast RISC rates for **DSBN** (74%, 1.03×10^6 s^{-1}) and **DSeBN** (84%, 1.98×10^6 s^{-1}), respectively. Furthermore, both the solution-processed and vacuum-evaporated OLEDs were fabricated by using **DSBN** and **DSeBN** as the emitter, demonstrating high maximum EQEs of 26.8% and 31.31% for solution-processed OLEDs, 32.08% and 35.31% for vacuum-evaporated OLEDs, respectively. Impressively, significantly suppressed efficiency roll-offs were figured out in vacuum-evaporated OLEDs, especially in **DSeBN**-based OLED, in which the EQE still maintained at 32.47% and 25.05% at the luminance of 100 and 1000 cd m^{-2}, respectively, attributing to the ultrafast RISC rate for the suppressed triplet-related annihilation processes.

2. Results and Discussion

2.1. Molecular Design and Characterization

The molecular design is illustrated in **Figure 1**. By integrating heavy atoms (S and Se) into the MR unit, significantly enhanced SOC matrix elements between different excited states were obtained for the fast spin-flip process of excitons. Therefore, the efficiency roll-offs of the EL devices would be much suppressed at the high current density. Meanwhile, the fusion of S/Se-B-N MR unit enhances the rigidity of molecular framework to reduce structural relaxation upon the excitation-emission process for the extremely narrow emission profile. Moreover, six methyl groups were introduced to improve the solubility and aggregation effect which are the common problems of rigid MR-TADF molecules encountered. As the proof-of-concept molecules, **DSBN** and **DSeBN** were synthesized with a good total yield by one-shot lithium-free borylation reaction. The detailed synthetic procedures of **DSBN** and **DSeBN** are depicted in Scheme S1 (Supporting Information). All intermediates and final products were fully confirmed by ^1H and ^{13}C NMR spectroscopy (Figures S1–S4, Supporting Information). Moreover, the final MR-TADF molecules of **DSBN** and **DSeBN** were further characterized by MALDI-TOF mass spectroscopy (Figures S5 and S6, Supporting Information). Their thermal properties were characterized by thermogravimetric analysis (TGA), demonstrating that both of them have a high decomposition temperatures (T_d) over 430 °C (Figure S7, Supporting Information), which are high enough for the stable device operation.

2.2. Photophysical Properties

To understand the fundamental effect of heavy atoms on the photophysical properties of MR-TADF molecules, the UV–vis absorption and steady-state photoluminescence (PL) spectra in dilute toluene solution were investigated first (**Table 1**). **DSBN** and **DSeBN** showed the similar absorption patterns with a series of electronic absorption bands, but **DSeBN** showed stronger intramolecular charge transfer (ICT) absorption peaking at 463 nm relative to the ones of n-π^* and π-π^* transitions (300-440 nm) than those for **DSBN** (**Figure 2a**), due to the stronger electron-donating ability of Se than that for S. This ICT character can be further confirmed by the solvatochromism experiment, where the absorption bands are red-shifted with the increase of solvent polarity (Figure S8, Supporting Information).[29] Moreover, both **DSBN** and **DSeBN** exhibited a sky-blue emission with a maximum peak at 472 and 473 nm (Figure 2b), as well as an extremely narrow FWHM value of 18 and 16 nm, respectively. Notably, **DSeBN** achieved the narrowest value of all the reported MR-TADF molecules containing the Se atom, due to the enhanced molecular rigidity by the further fusion of Se-B-N MR unit.[28,30] In addition, the high photoluminescence yields (PLQYs) of 95% for **DSBN** and 98% for **DSeBN** were found in the degassed toluene solution, indicating their high application potential in high-performance EL devices.

To study the TADF properties of **DSBN** and **DSeBN**, the PL and phosphorescence (Phos.) spectra were tested in toluene at 77 K. The small ΔE_{ST} values of 0.10 and 0.09 eV can be estimated from the onset of these spectra for **DSBN** and **DSeBN** (Figure 2c), respectively. With such small ΔE_{ST} and the enhanced SOC values owing to the heavy-atom effect, efficient spin-flip process of excitons would be anticipated. Then, the PL and transient lifetime decay characteristics of the doped film (2 wt%) in the host of 1,3-di(9*H*-carbazol-9-yl)benzene (*m*CP) were studied.

© 2024 The Author(s). Advanced Optical Materials published by Wiley-VCH GmbH

21951071, 2024, 25, Downloaded from https://onlinelibrary.wiley.com/doi/10.1002/adom.202400794 by Hong Kong Poly University, Wiley Online Library on [13/09/2024]. See the Terms and Conditions (https://onlinelibrary.wiley.com/terms-and-conditions) on Wiley Online Library for rules of use; OA articles are governed by the applicable Creative Commons License

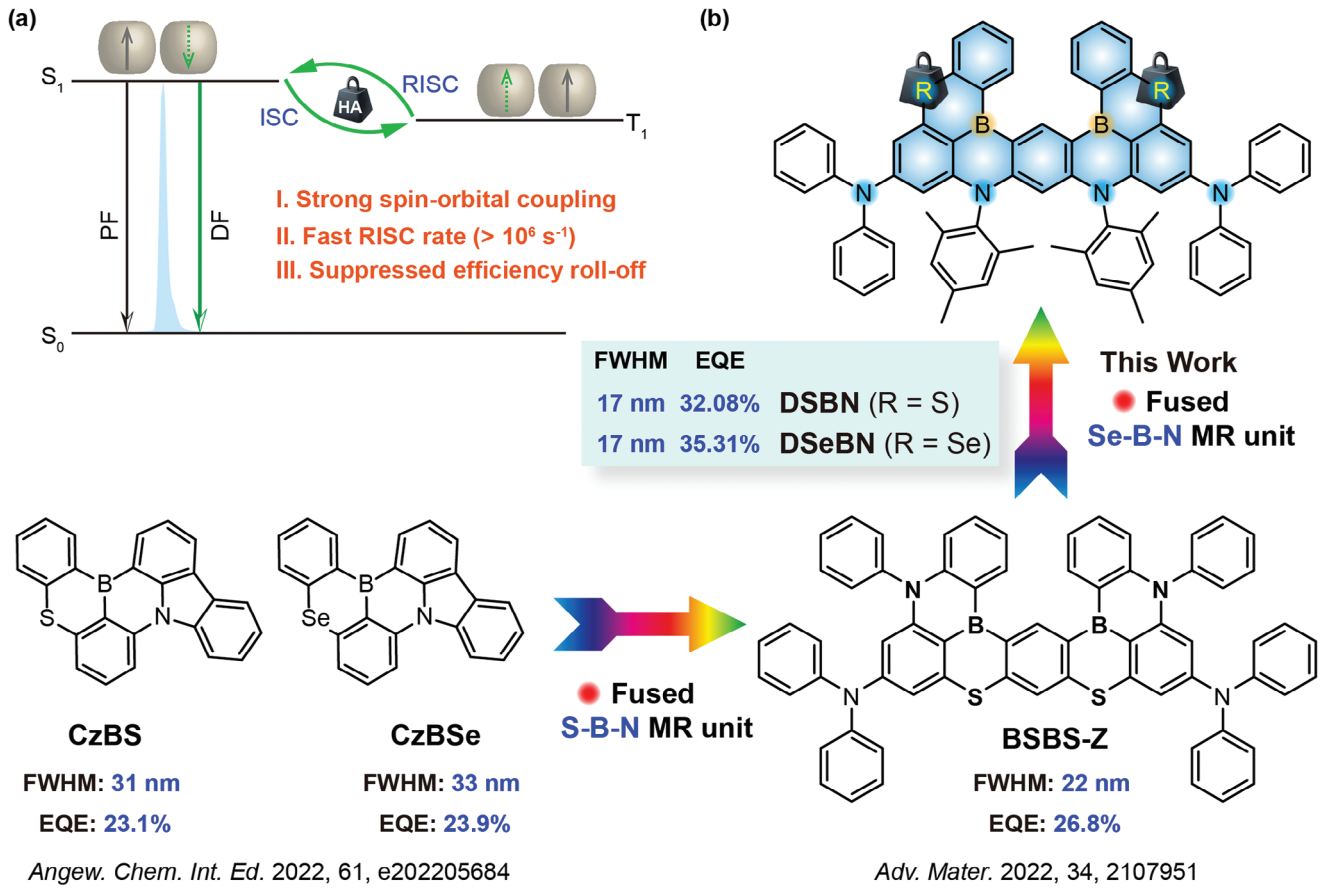

Figure 1. a) The scheme of heavy-atom (HA) effect for the enhanced RISC process in TADF molecules. b) Molecular design of MR-TADF molecules doped with heavy atoms.

The maximum emission peaks of 481 and 482 nm, as well as a narrow FWHM of 18 nm were found in the doped films of **DSBN** and **DSeBN**, respectively, due to the fused and rigid molecular skeleton. Moreover, these two molecules showed unobvious bathochromic shift and broadening of emission spectra with the increase of doping concentration, because of the suppressed aggregation effect by the steric hindrance of six methyl groups introduced (Figure S9, Supporting Information).[31,32] The lifetime decay curves were tested to directly confirm the TADF properties of **DSBN** and **DSeBN**. The prompt fluorescence (PF) and delayed fluorescence (DF) lifetimes of **DSBN** doped film are 1.59 ns and 1.36 µs (Figure 2d), respectively, in which the short DF lifetime indicates the faster RISC process of **DSBN** than those of most reported MR-TADF molecules. Impressively, because of more efficient heavy-atom effect of Se atom, **DSeBN** exhibits shorter PF and DF lifetimes than those for **DSBN**, being 0.74 ns and 0.52 µs, respectively, which are the shortest lifetimes among all the reported MR-TADF molecules.[9,20] Such short DF lifetime is conducive to the fast spin flipping of exctions for the significantly suppressed efficiency roll-off at high current density of EL device. Moreover, PLQYs of **DSBN** and **DSeBN** doped films were measured to be 93% and 95%, respectively. High DF efficiencies were figured out to be 74% and 84%, respectively, which are much higher than those for the N-B-N analogue of *ν*-DABNA owing to the heavy atom promoted RISC process (Figure 2e).[33] Based on the PLQYs and lifetimes, the key rate constants were calculated (Figure 2f). **DSBN** and **DSeBN** showed fast singlet radiative transition rates (k_r) of 1.19×10^8 and 1.49×10^8 s^{-1}, respectively. Obviously, fast intersystem crossing rates (k_{ISC}) and RISC rates (k_{RISC}) were evaluated for the doped films of **DSBN** (4.18×10^8

Table 1. Photophysical parameters of **DSBN** and **DSeBN**.

Emitter	λ_{abs} [a] [nm]	λ_{PL} [a] [nm]	FWHM [nm]	ΔE_{ST} [b] [eV]	ϕ_{PL} [a/c]	τ_p [c] [ns]	τ_d [c] [µs]	k_r [10^8 s^{-1}]	k_{ISC} [10^8 s^{-1}]	k_{RISC} [10^6 s^{-1}]	HOMO [eV]	LUMO [eV]	CIE [a] [x, y]
DSBN	463	472	18	0.10	0.95/0.93	1.59	1.36	1.19	4.18	1.03	−5.17	−2.57	0.116, 0.108
DSeBN	464	473	16	0.09	0.98/0.95	0.74	0.52	1.49	11.3	1.98	−5.16	−2.57	0.110, 0.133

[a] Measured in dilute toluene (10^{-5} mol L^{-1}); [b] Determined from the onset of the fluorescence and phosphorescence spectra at 77 K in dilute toluene (10^{-5} mol L^{-1}); [c] Measured in doped films (2 wt% **DSBN**/**DSeBN** in mCP).

© 2024 The Author(s). Advanced Optical Materials published by Wiley-VCH GmbH

21951071, 2024, 25, Downloaded from https://onlinelibrary.wiley.com/doi/10.1002/adom.202400794 by Hong Kong Poly University, Wiley Online Library on [13/09/2024]. See the Terms and Conditions (https://onlinelibrary.wiley.com/terms-and-conditions) on Wiley Online Library for rules of use; OA articles are governed by the applicable Creative Commons License

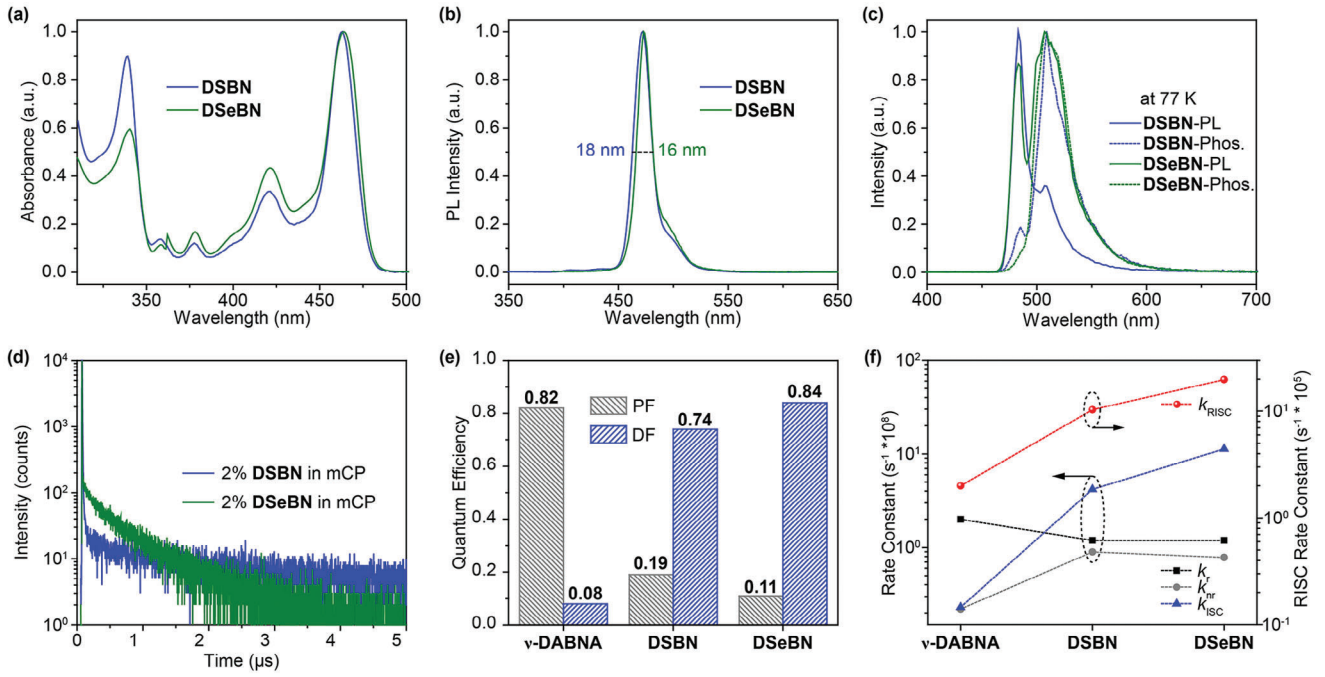

Figure 2. a) UV–vis absorption and b) steady-state photoluminescence (PL) spectra of **DSBN** and **DSeBN** in dilute toluene (10^{-5} mol L^{-1}). c) PL and phosphorescence (Phos.) spectra of **DSBN** and **DSeBN** in dilute toluene at 77 K. d) Lifetime decay curves of **DSBN** and **DSeBN** doped films. e) The comparison of PLQYs of *ν*-DABNA, **DSBN** and **DSeBN** in doped films. f) The calculated key rate constants of *ν*-DABNA, **DSBN** and **DSeBN** doped films.

and 1.03×10^6 s^{-1}) and **DSeBN** (1.13×10^9 and 1.98×10^6 s^{-1}), respectively, and these values are much higher than those of most reported MR-TADF emitters owing to the enhanced SOC matrix elements between the excited singlet and triplet states by the heavy-atom effect.

2.3. Theoretical Calculations

To understand the electronic properties of **DSBN** and **DSeBN**, the density functional theory (DFT) and time dependent-DFT (TD-DFT) calculations were performed. As shown in **Figure** 3a, a large portion of HOMOs is located at the nitrogen atom and at the *meta* position relative to the boron atom inside the MR unit, but a small part of HOMOs is distributed on the strong electron-donating diphenylamine group. Meanwhile, the LUMOs are mainly localized on the boron atom and the *ortho* and *para* positions of it inside the MR unit, resulting in a hybrid short- and long-range charge transfer process, which is probably conducive to enhance the TADF characteristics.[34,35] Moreover, the SOC matrix elements were simulated (Figure 3b; Table S1, Supporting Information). A small energy gap between singlet and triplet excited states of 0.10 and 0.09 eV in experiment for **DSBN** and **DSeBN**, as well as a large SOC were found between T_n (n = 1–4) and S_1. As expected, **DSeBN** showed enhanced SOC values compared to the ones of **DSBN**, indicating the efficient heavy-atom effect of Se atom. Moreover, the SOC between S_1 and T_2 is larger than that between S_1 and T_1, confirming that it is the T_2 state, which may be mixed with the T_1 state via the "ΔE_{ST} matching" vibrational mode, that probably enhances the spin-vibronic coupling (SVC)-assisted RISC process.[35–38]

The electrochemical properties of **DSBN** and **DSeBN** were tested by cyclic voltammetry (CV) measurements (Figure S11, Supporting Information). The similar HOMO energy levels were figured out from the onset of the oxidation wave, being −5.17 and −5.16 eV for **DSBN** and **DSeBN**, respectively. The LUMO energy levels were calculated to be −2.57 eV for both of them, indicating that the incorporation of S and Se atoms would selectively modulate the photophysical properties of MR-TADF molecules without affecting their electrochemical properties.

2.4. Electroluminescence Performances

Inspired by the excellent solubilities, narrowband emissions and highly efficient TADF properties of **DSBN** and **DSeBN**, the solution-processed OLEDs were fabricated first (**Figure** 4a) by using the device configuration of ITO/PEDOT:PSS (40 nm)/EML (40 nm)/DPEPO (10 nm)/TmPyPB (50 nm)/LiF (1 nm)/Al (120 nm), in which Al and indium tin oxide (ITO) served as the cathode and anode, respectively; poly(3,4-ethylenedioxythiophene):poly(styrene sulfonic acid) (PEDOT:PSS) and LiF acted as hole- and electron-injecting materials, respectively; 1,3,5-tri(m-pyrid-3-yl-phenyl)-benzene (TmPyPB) was chosen as electron-transporting material; bis[2-(diphenylphosphino)phenyl]ether oxide (DPEPO) performed the function of exciton-blocking layer; *m*CP was employed as the host material. The doping concentration was finely regulated to realize the best performance (Figures S12 and S13; Tables S2 and S3, Supporting Information).

As displayed in Figures 4b–d, the solution-processed OLEDs based on **DSBN** (**SP-DSBN**) and **DSeBN**(**SP-DSeBN**) showed

© 2024 The Author(s). Advanced Optical Materials published by Wiley-VCH GmbH

21951071, 2024, 25, Downloaded from https://onlinelibrary.wiley.com/doi/10.1002/adom.202400794 by Hong Kong Poly University, Wiley Online Library on [13/09/2024]. See the Terms and Conditions (https://onlinelibrary.wiley.com/terms-and-conditions) on Wiley Online Library for rules of use; OA articles are governed by the applicable Creative Commons License

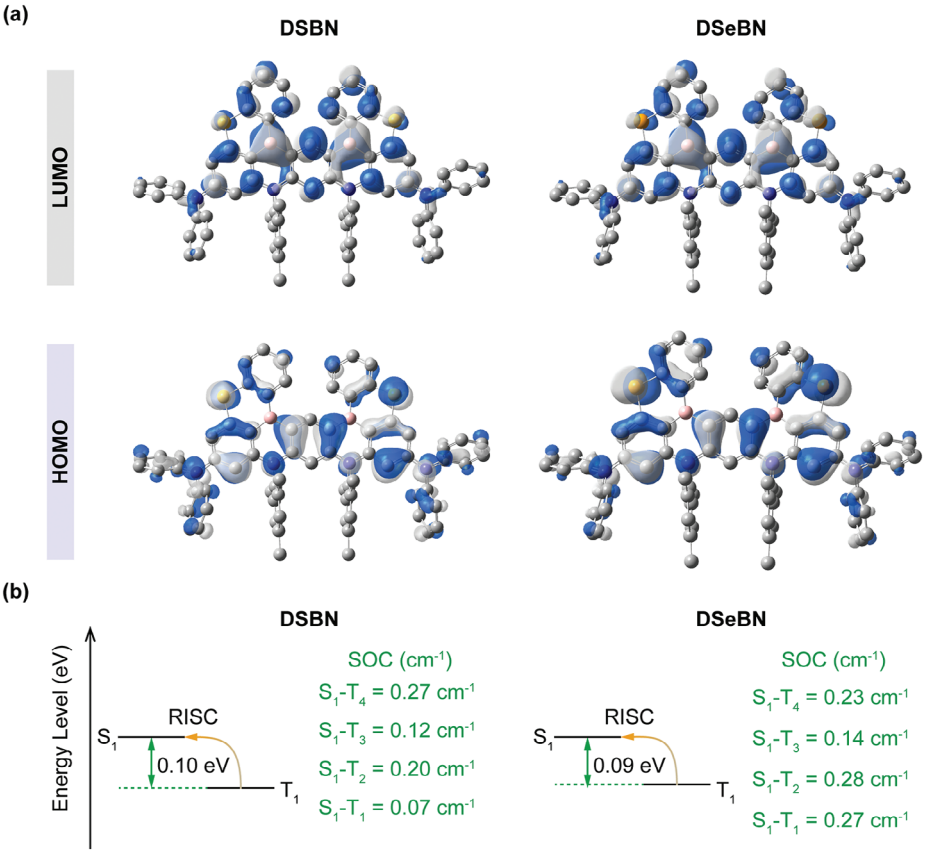

Figure 3. a) Calculated HOMO and LUMO distributions. b) Energy level diagrams in experiment and associated SOC matrix elements between S_1 and T_n (n = 1–4).

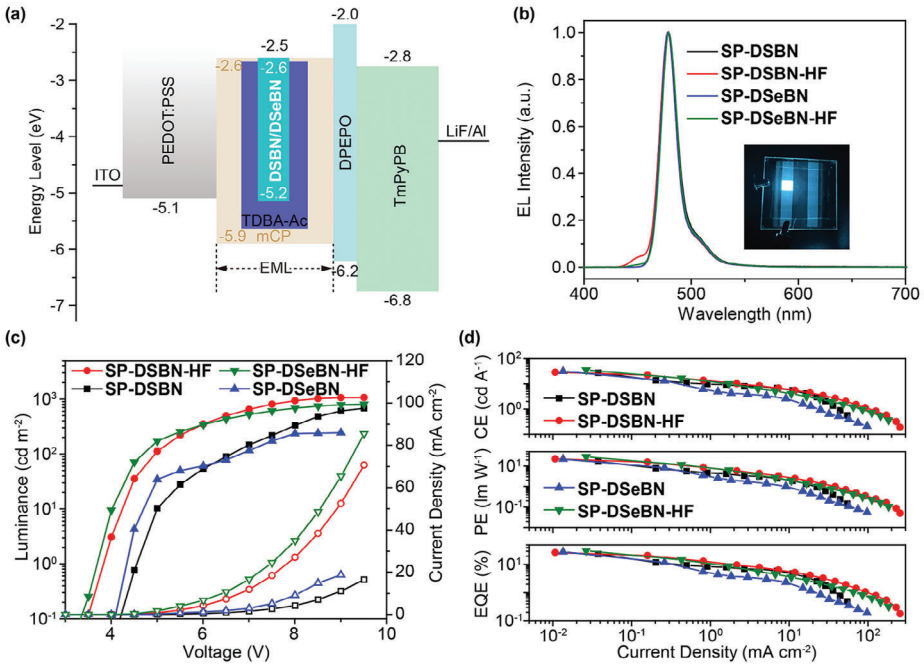

Figure 4. a) The device configuration and the energy level diagram of solution-processed OLEDs. b) Electroluminescence spectra (inset is the image of operating device of **DSeBN** under 6 V). c) Luminance-voltage-current density and d) efficiency-luminance curves of OLEDs based on **DSBN** and **DSeBN** as the emitter, respectively.

© 2024 The Author(s). Advanced Optical Materials published by Wiley-VCH GmbH

21951071, 2024, 25, Downloaded from https://onlinelibrary.wiley.com/doi/10.1002/adom.202400794 by Hong Kong Poly University, Wiley Online Library on [13/09/2024]. See the Terms and Conditions (https://onlinelibrary.wiley.com/terms-and-conditions) on Wiley Online Library for rules of use; OA articles are governed by the applicable Creative Commons License

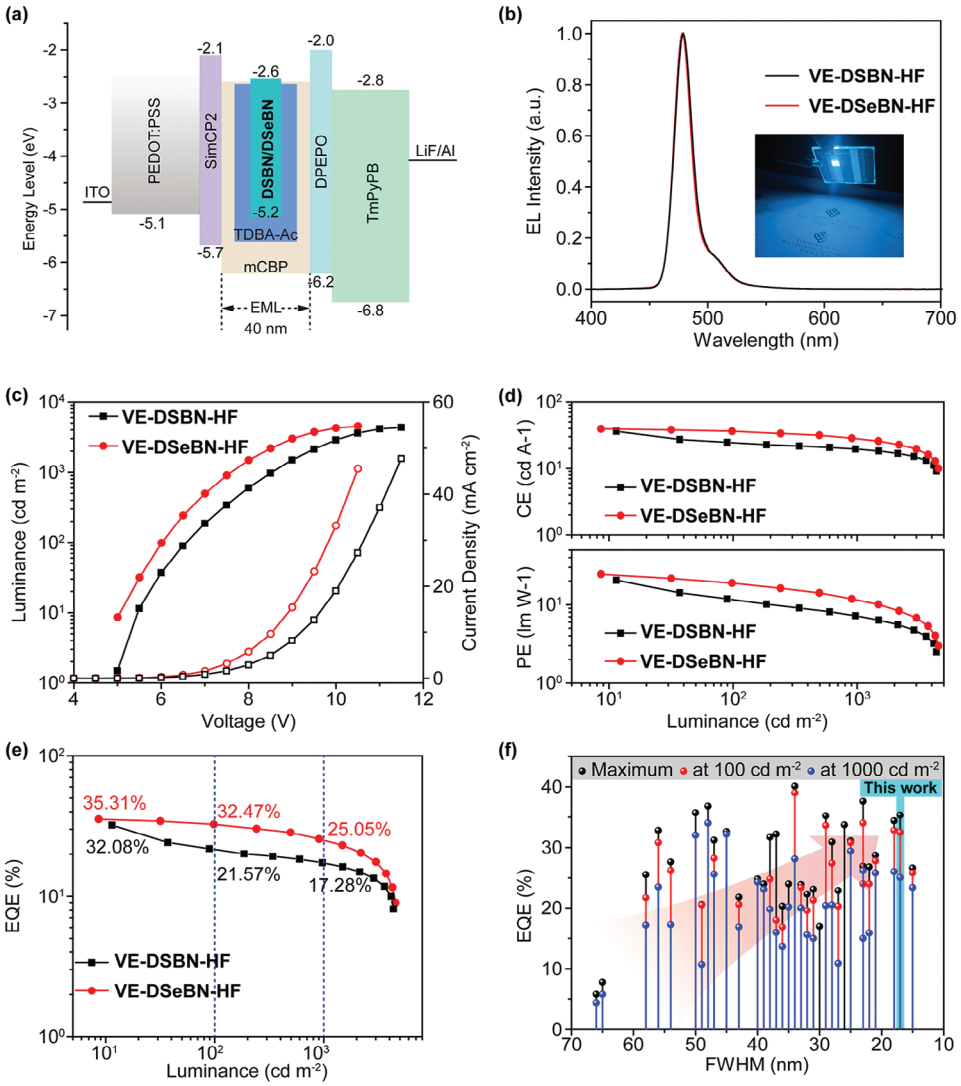

Figure 5. a) The device configuration and the energy level diagram of vacuum-evaporated OLEDs. b) Electroluminescence spectra of **DSBN**- and **DSeBN**-based OLEDs. Inset is the lighting image of PolyU logo by an operating device of **DSeBN**. c) Luminance-voltage-current density and d,e) efficiency-luminance curves of blue OLEDs based on **DSBN** and **DSeBN** as the emitter. f) Summary of EQE versus FWHM of OLEDs based on reported narrowband emitters.

pure sky-blue emissions with an emission peak at 478 nm and a narrow FWHM value of 18 nm for **DSBN** and 17 nm for **DSeBN**, which are consistent with the characteristics of PL, demonstrating the good energy transfer from *m*CP to guests in the EL process. Moreover, **DSBN**-based OLED achieved a good performance with a maximum EQE of 23.5%, a maximum current efficiency (CE) of 27.0 cd A^{-1} and a maximum power efficiency (PE) of 17.0 lm W^{-1}. Because of the higher PLQY of **DSeBN** relative to **DSBN**, OLED based on **DSeBN** achieved a higher maximum EQE up to 28.6%. Furthermore, solution-processed hyperfluorescence devices based on **DSBN** (**SP-DSBN-HF**) and **DSeBN** (**SP-DSeBN-HF**) as the emitters were further constructed to realize the full utilization of excitons. The TADF sensitizer is TDBA-Ac, which has been reported with a high S_1/T_1 of 3.11/3.05 eV and a fast RISC rate of 0.99×10^6 s^{-1}.[39] Moreover, TDBA-Ac has a suitable spectral overlap between its emission and the absorption spectra of **DSBN** and **DSeBN**. As expected, much improved performances were obtained in these devices, with a reduced turn-on voltage and a higher maximum EQE for **DSBN** (3.8 V and 26.8%) and **DSeBN** (3.8 V and 31.3%), respectively. These results demonstrate a record-high performance of solution-processed blue MR-TADF OLEDs.[40,41]

Although the solution-processed OLEDs based on **DSBN** and **DSeBN** achieved high efficiencies, the large efficiency roll-offs were found, probably due to the improper device configuration that caused the leakage of excitons. To avoid this issue and reveal the impact of heavy atoms on the suppression of efficiency roll-off, a exciton-blocking layer of bis[3,5-di(9*H*-carbazol-9-yl)phenyl]diphenylsilane (SimCP2) was added to fabricate the vacuum-evaporated hyperfluorescence devices based on 3,3′-di(9*H*-carbazol-9-yl)−1,1′-biphenyl (*m*CBP) as the host material (**Figure 5a**), the optimized EML concentration is 3 wt%

© 2024 The Author(s). Advanced Optical Materials published by Wiley-VCH GmbH

21951071, 2024, 25, Downloaded from https://onlinelibrary.wiley.com/doi/10.1002/adom.202400794 by Hong Kong Poly University, Wiley Online Library on [13/09/2024]. See the Terms and Conditions (https://onlinelibrary.wiley.com/terms-and-conditions) on Wiley Online Library for rules of use; OA articles are governed by the applicable Creative Commons License

Table 2. Summarized EL performance data of vacuum-evaporated OLEDs based on **DSBN** and **DSeBN**.

Devices	L_{max} [a] [cd m^{-2}]	λ_{em} [b] [nm]	FWHM [c] [nm]	$EQE_{max,\ 100,\ 1000}$ [d] [%]	CE_{max} [e] [cd A^{-1}]	PE_{max} [f] [lm W^{-1}]	CIE [g] [x, y]
VE-DSBN-HF	4353	478	17	32.08, 21.57, 17.28	36.08, 24.24, 19.42	20.62, 11.58, 7.16	0.098, 0.188
VE-DseBN-HF	4524	478	17	35.31, 32.47, 25.05	39.15, 36.07, 27.77	24.59, 18.81, 11.49	0.099, 0.182

[a] The maximum luminance; [b] EL emission peak at the voltage of 6 V; [c] Full width at half maximum of the EL spectrum; [d] The maximum EQE and the EQEs measured at 100 and 1000 cd m^{-2}; [e] Maximum current efficiency and the CEs measured at 100 and 1000 cd m^{-2}; [f] Maximum power efficiency and the PEs measured at 100 and 1000 cd m^{-2}; [g] CIE chromaticity coordinates recorded at the voltage of 6 V.

DSBN or **DSeBN**:10 wt% TDBA-Ac, named as **VE-DSBN-HF** and **VE-DSeBN-HF**, respectively. Both of them exhibited extremely pure blue EL with a sharp emission peak at 478 nm and a narrow FWHM of 17 nm (Figure 5b, **Table 2**). These devices have a good color stability with the stable EL spectra over a wide range of voltages (Figure S15, Supporting Information). Moreover, excellent performances were achieved in these two devices (Figures 5c,d), with a high maximum EQE up to 32.1% and 35.3% for **VE-DSBN-HF** and **VE-DSeBN-HF**, respectively. Impressively, the efficiency roll-offs were much suppressed owing to the fast RISC rates of **DSBN** and **DSeBN**. Especially in **DSeBN**-based device, the EQE still maintained at 32.47% and 25.05% at the luminance of 100 (for display) and 1000 cd m^{-2} (for lighting), respectively. These results represent the state-of-the-art performance of MR-TADF-based OLEDs in terms of FWHM and EQE (Figure 5f; Table S4, Supporting Information).[9]

3. Conclusion

In summary, a design strategy was proposed by the fusion of MR unit with the heavy atoms (S and Se) to achieve narrowband emission and speed up the RISC process simultaneously for high-performance MR-TADF molecules. As prepared molecules, **DSBN** and **DSeBN** exhibited extremely narrow FWHM values and much enhanced DF emission. Especially for the Se-embedded emitter (**DSeBN**), the FWHM was only 16 nm and the shortest DF lifetime of 0.56 µs was achieved among all the reported TADF molecules, because of the rigid molecular framework and heavy-atom effect. Such large RISC rate constant of 1.98×10^6 s^{-1} was obtained, which is conducive to the fast spin-conversion process of excitons for significantly suppressed efficiency roll-off. Impressively, the excellent performances were achieved both in solution-processed and vacuum-evaporated OLEDs, with a maximum EQE up to 26.8% and 32.1% for **DSBN**-based OLEDs, 31.3% and 35.3% for **DSeBN**-based OLEDs, respectively. Significantly, **DSeBN**-based vacuum-evaporated OLEDs showed extremely narrow FWHM of 17 nm and much suppressed efficiency roll-off, in which the EQEs still stayed at 32.47% and 25.05% at the luminance of 100 and 1000 cd m^{-2}, respectively, representing the state-of-the-art performance of the blue OLEDs in terms of EQE and FWHM. This work demonstrates a feasible molecular design and represents an important step toward achieving high-performance MR-TADF molecules with both narrowband emission and low efficiency roll-off.

Supporting Information

Supporting Information is available from the Wiley Online Library or from the author.

Acknowledgements

J.J. and M.C. contributed equally to this work. This work was supported by the National Key R & D Program of China (2022YFE0104100), the National Natural Science Foundation of China (22205188), ITC Guangdong-Hong Kong Technology Cooperation Funding Scheme (TCFS) (GHP/038/19GD), CAS-Croucher Funding Scheme for Joint Laboratories (ZH4A), the Hong Kong Research Grants Council (PolyU 15305320), the Hong Kong Polytechnic University (YXB8), Miss Clarea Au for the Endowed Professorship in Energy (847S), Research Institute for Smart Energy (CDAQ) and Open Research Fund of State Key Laboratory of Polymer Physics and Chemistry, Changchun Institute of Applied Chemistry, Chinese Academy of Sciences (No. 2020-17). B. Z. was supported by the Natural Science Foundation of Guangdong Province (2021A1515010510, 2023A1515010053), Science and Technology Projects in Guangzhou (No.202201000002, 202102010409), Department of Science & Technology of Guangdong Province (ID: 2022A156), Key Discipline of Materials Science and Engineering, Bureau of Education of Guangzhou (No. 20225546), and Open Research Fund of State Key Laboratory of Polymer Physics and Chemistry, Changchun Institute of Applied Chemistry, Chinese Academy of Sciences (No. 2022-12).

Conflict of Interest

The authors declare no conflict of interest.

Data Availability Statement

The data that support the findings of this study are available from the corresponding author upon reasonable request.

Keywords

heavy-atom effect, multi-resonance thermally activated delayed fluorescence, narrowband emission, organic light-emitting diodes

Received: March 22, 2024
Revised: June 22, 2024
Published online: July 27, 2024

[1] H. Uoyama, K. Goushi, K. Shizu, H. Nomura, C. Adachi, *Nature* **2012**, *492*, 234.

© 2024 The Author(s). Advanced Optical Materials published by Wiley-VCH GmbH

21951071, 2024, 25, Downloaded from https://onlinelibrary.wiley.com/doi/10.1002/adom.202400794 by Hong Kong Poly University, Wiley Online Library on [13/09/2024]. See the Terms and Conditions (https://onlinelibrary.wiley.com/terms-and-conditions) on Wiley Online Library for rules of use; OA articles are governed by the applicable Creative Commons License

[2] A. Endo, M. Ogasawara, A. Takahashi, D. Yokoyama, Y. Kato, C. Adachi, *Adv. Mater.* **2009**, *21*, 4802.
[3] Y. Liu, C. Li, Z. Ren, S. Yan, M. R. Bryce, *Nat. Rev. Mater.* **2018**, *3*, 18020.
[4] L. S. Cui, A. J. Gillett, S. F. Zhang, H. Ye, Y. Liu, X. K. Chen, Z. S. Lin, E. W. Evans, W. K. Myers, T. K. Ronson, H. Nakanotani, S. Reineke, J. L. Bredas, C. Adachi, R. H. Friend, *Nat. Photonics* **2020**, *14*, 636.
[5] Y. Wada, H. Nakagawa, S. Matsumoto, Y. Wakisaka, H. Kaji, *Nat. Photonics* **2020**, *14*, 643.
[6] X. Tang, L. S. Cui, H. C. Li, A. J. Gillett, F. Auras, Y. K. Qu, C. Zhong, S. T. E. Jones, Z. Q. Jiang, R. H. Friend, L. S. Liao, *Nat. Mater.* **2020**, *19*, 1332.
[7] D. Karthik, Y. H. Jung, H. Lee, S. Hwang, B. M. Seo, J. Y. Kim, C. W. Han, J. H. Kwon, *Adv. Mater.* **2021**, *33*, 2007724.
[8] K. Wang, C. J. Zheng, W. Liu, K. Liang, Y. Z. Shi, S. L. Tao, C. S. Lee, X. M. Ou, X. H. Zhang, *Adv. Mater.* **2017**, *29*, 1701476.
[9] H. Jiang, J. Jin, W. Y. Wong, *Adv. Funct. Mater.* **2023**, *33*, 2306880.
[10] Y. Tao, K. Yuan, T. Chen, P. Xu, H. Li, R. Chen, C. Zheng, L. Zhang, W. Huang, *Adv. Mater.* **2014**, *26*, 7931.
[11] M. Y. Wong, E. Zysman-Colman, *Adv. Mater.* **2017**, *29*, 1605444.
[12] T. Zhang, Y. Xiao, H. Wang, S. Kong, R. Huang, V. K. Au, T. Yu, W. Huang, *Angew. Chem., Int. Ed.* **2023**, *135*, 202301896.
[13] T. Hatakeyama, K. Shiren, K. Nakajima, S. Nomura, S. Nakatsuka, K. Kinoshita, J. Ni, Y. Ono, T. Ikuta, *Adv. Mater.* **2016**, *28*, 2777.
[14] X. C. Fan, K. Wang, Y. Z. Shi, Y. C. Cheng, Y. T. Lee, J. Yu, X. K. Chen, C. Adachi, X. H. Zhang, *Nat. Photonics* **2023**, *17*, 280.
[15] J. Liu, Y. Zhu, T. Tsuboi, C. Deng, W. Lou, D. Wang, T. Liu, Q. Zhang, *Nat. Commun.* **2022**, *13*, 4876.
[16] Y. Y. Jing, N. Li, X. Cao, H. Wu, J. Miao, Z. Chen, M. Huang, X. Wang, Y. Hu, Y. Zou, C. Yang, *Sci. Adv.* **2023**, *9*, eadh8296.
[17] Y. Sano, T. Shintani, M. Hayakawa, S. Oda, M. Kondo, T. Matsushita, T. Hatakeyama, *J. Am. Chem. Soc.* **2023**,*145*, 11504.
[18] M. Yang, I. S. Park, T. Yasuda, *J. Am. Chem. Soc.* **2020**, *142*, 19468.
[19] H. J. Kim, T. Yasuda, *Adv. Opt. Mater.* **2022**, *10*, 2201714.
[20] K. R. Naveen, H. I. Yang, J. H. Kwon, *Commun. Chem.* **2022**, *5*, 149.
[21] X. Fan, X. Hao, F. Huang, J. Yu, K. Wang, X. Zhang, *Adv. Sci.* **2023**, *10*, 2303504.
[22] S. M. Pratik, V. Coropceanu, J. L. Brédas, *Chem. Mater.* **2022**, *34*, 8022.
[23] J. Wang, N. Li, C. Zhong, J. Miao, Z. Huang, M. Yu, Y. X. Hu, S. Luo, Y. Zou, K. Li, C. Yang, *Adv. Mater.* **2022**, *35*, 2208378.
[24] Y. Hu, J. Miao, C. Zhong, Y. Zeng, S. Gong, X. Cao, X. Zhou, Y. Gu, C. Yang, *Angew. Chem., Int. Ed.* **2023**, *62*, 202302478.
[25] S. Pratik, V. Coropceanu, J. L. Brédas, *ACS Mater. Lett.* **2022**, *4*, 440.
[26] Y. X. Hu, J. Miao, T. Hua, Z. Huang, Y. Qi, Y. Zou, Y. Qiu, H. Xia, H. Liu, X. Cao, C. Yang, *Nat. Photonics* **2022**, *16*, 803.
[27] I. S. Park, H. Min, T. Yasuda, *Angew. Chem., Int. Ed.* **2022**, *61*, 202205684.
[28] I. S. Park, M. Yang, H. Shibata, N. Amanokura, T. Yasuda, *Adv. Mater.* **2022**, *34*, 2107951.
[29] J. Jin, C. Duan, H. Jiang, P. Tao, H. Xu, W. Y. Wong, *Angew. Chem., Int. Ed.* **2023**, *62*, 202218947.
[30] Q. Li, Y. Wu, Q. Yang, S. Wang, S. Shao, L. Wang, *ACS Appl. Mater. Interfaces* **2022**, *34*, 2106954.
[31] P. Jiang, J. Miao, X. Cao, H. Xia, K. Pan, T. Hua, X. Lv, Z. Huang, Y. Zou, C. Yang, *Adv. Mater.* **2022**, *34*, 2106954.
[32] Y. Zhang, J. Wei, D. Zhang, C. Yin, G. Li, Z. Liu, X. Jia, J. Qiao, L. Duan, *Angew. Chem., Int. Ed.* **2022**, *61*, 202113206.
[33] Y. Kondo, K. Yoshiura, S. Kitera, H. Nishi, S. Oda, H. Gotoh, Y. Sasada, M. Yanai, T. Hatakeyama, *Nat. Photonics* **2019**, *13*, 678.
[34] G. Meng, H. Dai, Q. Wang, J. Zhou, T. Fan, X. Zeng, X. Wang, Y. Zhang, D. Yang, D. Ma, D. Zhang, L. Duan, *Nat. Commun.* **2023**, *14*, 2394.
[35] H. L. Lee, J. Kang, J. Lim, S. C. Kim, S. O. Jeon, J. Y. Lee, *Nat. Commun.* **2023**, *14*, 4818.
[36] H. J. Cheon, S. J. Woo, S. H. Baek, J. H. Lee, Y. H. Kim, *Adv. Mater.* **2022**, *34*, 2207416.
[37] S. Oda, B. Kawakami, Y. Yamasaki, R. Matsumoto, M. Yoshioka, D. Fukushima, S. Nakatsuka, T. Hatakeyama, *J. Am. Chem. Soc.* **2021**, *144*, 106.
[38] I. Kim, K. H. Cho, S. O. Jeon, W. J. Son, D. Kim, Y. M. Rhee, I. Jang, H. Choi, D. S. Kim, *JACS Au* **2021**, *1*, 987.
[39] D. H. Ahn, S. W. Kim, H. Lee, I. J. Ko, D. Karthik, J. Y. Lee, J. H. Kwon, *Nat. Photonics* **2019**, *13*, 540.
[40] T. Wang, X. Yin, X. Cao, C. Yang, *Angew. Chem., Int. Ed.* **2023**, *62*, 202301988.
[41] T. Wang, Y. Zou, Z. Huang, N. Li, J. Miao, C. Yang, *Angew. Chem., Int. Ed.* **2022**, *61*, 202211172.

© 2024 The Author(s). Advanced Optical Materials published by Wiley-VCH GmbH

21951071, 2024, 25, Downloaded from https://onlinelibrary.wiley.com/doi/10.1002/adom.202400794 by Hong Kong Poly University, Wiley Online Library on [13/09/2024]. See the Terms and Conditions (https://onlinelibrary.wiley.com/terms-and-conditions) on Wiley Online Library for rules of use; OA articles are governed by the applicable Creative Commons License